Temperature effect on dynamic wetting of cellulosic substrates by molten polymers for composite processing

Monica Francesca Pucci, Benoît Duchemin, Moussa Gomina, Joël Bréard

Temperature effect on dynamic wetting of cellulosic substrates by molten polymers for composite processing

Monica Francesca Pucci[a,c,*], Benoît Duchemin[b], Moussa Gomina[a], Joël Bréard[b]

[a] CRISMAT, UMR 6508 CNRS, ENSICAEN, 6 Boulevard Maréchal Juin, 14050 Caen Cedex 4, France [b] LOMC, UMR 6294 Université du Havre, 53 rue de Prony, 76058 Le Havre, France [c] C2MA, IMT Mines Alès, Univ Montpellier, 6 Avenue de Clavières, 30100 Alès, France[1]

Keywords:
A. Cellulose
B. Surface properties
B. Wettability
E. Liquid composite moulding

ABSTRACT

Impregnation of plant fibre reinforcements by a molten polymer involves many phenomena still poorly understood, related to the solid morphology and its surface chemistry, but also to the temperature effect on liquid properties and solid/liquid interactions. The present work focuses on the temperature effect on forced dynamic wetting, using the Wilhelmy method and two model materials: a cellulosic film and two totally wetting paraffin oils. The results show that the dynamic contact angle vs. the capillary number (Ca) plot appears as a master curve. This curve is split in two domains. The domain associated with $Ca>10^{-3}$ is well described by the hydrodynamic approach. The domain with $Ca<10^{-3}$ corresponds to wetting processes operating on a smaller scale, which are more sensitive to the physico-chemical heterogeneities of the substrate. This study addresses the mechanisms governing the capillary pressure, void formation and interface generation during composite manufacturing.

Preprint version of : Pucci, M.F., Duchemin, B., Gomina, M., Bréard, J., 2018. Temperature effect on dynamic wetting of cellulosic substrates by molten polymers for composite processing. Composites Part A: Applied Science and Manufacturing 114, 307–315. https://doi.org/10.1016/j.compositesa.2018.08.031

*Corresponding author at: C2MA, IMT Mines Alès, Univ Montpellier, 6 Avenue de Clavières, 30100 Alès, France. E-mail address: monica.pucci@mines-ales.fr (M.F. Pucci). [1] Current affiliation.

1. Introduction

Current research in the field of composite materials aims at minimizing their environmental impact by carefully reassessing their life cycles. These environmental studies usually focus on three main contextual aspects: the life cycle of the individual materials, the energy efficiency of their manufacturing and the end-of-life fate of the composite materials. For obvious reasons, it can be advantageous to use biobased materials because of their renewability and ease of disposal. In that respect, cellulose and cellulosic materials (natural and man-made fibres, regenerated cellulosic films, nanopapers, etc.) have a natural advantage over most of their synthetic counterparts. Having a good control of (bio) composite manufacturing can also be pivotal with regard to energy efficiency and hidden energy costs (durability, specific mechanical properties). The polymers in question can belong to the three main polymer families, i.e. thermoplastics, rubbers or thermosets. It is known that capillary effects and particularly, capillary parameters like molten polymer surface tension and cellulose surface energy play an important role on substrate/matrix compatibility and fibre impregnation. Capillary forces coupled with the viscous ones play a dominant role in dynamic wetting during composite processing [1,2], that were expressed with the definition of the capillary pressure [3,4]. Moreover, a lot of experimental [5–9] and numerical [10,11] works mentioned that capillary and viscous effects lead to porosity formation, depending on local liquid velocity v in the heterogeneous fibrous preform and liquid properties, both included in the capillary number Ca:

$$Ca = \frac{\eta v}{\gamma_{LV}} \quad (1)$$

where η and γ_{LV} are respectively the dynamic viscosity and the liquid surface tension. Dynamic wetting phenomena are described by a dynamic contact angle between the liquid–vapour interface and the solid surface (θ_d) and it is well known that θ_d exhibits a strong dependence on Ca.

There are many studies about dynamic wetting models that aim at predicting wetting phenomena in different conditions and at different length scales, from the molecular to the macroscopic scale. Dynamic wetting concerns all phenomena in which the triple contact line between the liquid, the solid and the vapour phase moves forming a dynamic contact angle, that is different from the angle reached at the equilibrium state. θ_d can be an advancing contact angle (θ_a), when the triple contact line advances on the dry solid surface, or a receding contact angle (θ_r) when it recedes from the wetted surface [12]. By convention, v and Ca will have positive values in advancing case and negative ones in the receding case [13]. When referring to dynamic wetting, it is important to specify whether the evolution of the contact line is spontaneous or forced [14]. Spontaneous wetting occurs when the spreading of the liquid is driven only by the solid–liquid interactions. A typical example is the spontaneous capillary rise of a liquid in a tube or the liquid imbibition in a porous medium [15,16]. In contrast, forced wetting occurs when an externally imposed force drives the displacement of the triple line beyond its equilibrium. A daily example is that of a solid pulled out of a liquid with an imposed speed, such as a fibre continuously pulled out of a treatment bath [17].

Several dynamic wetting models describe the dependence of contact angles on the velocity of the moving contact line [18]. These models essentially fall into two categories: an hydrodynamic (HD) approach at a macro-mesoscopic scale and the molecular kinetic (MK) theory built on microscopic considerations. The former considers that the dissipation channel of dynamic wetting is viscous and occurs in the core of liquid, far from the moving contact line. The latter considers a microscopic dissipation due to molecular

displacements (local phenomena) in the vicinity of the contact line [19]. However, it was found that these two approaches work best in different Ca ranges: at "high" Ca (above ≈ 10^{-3}) the viscous dissipation dominates, and the HD approach fits well experimental results of wetting phenomena. On the contrary, "low" Ca (below ≈ 10^{-3}) are best described by the MK theory, since the molecular displacement dissipation at the triple line is prevalent at low speeds [20]. Combined models coupling the two dissipation channels were also derived [21], to provide equations describing the evolution of the dynamic contact angle in broader Ca ranges, but resulting in an important number of free parameters to determine, with the risk of loosing the physical significance of each parameter [22].

Experimentally, the majority of works dedicated to dynamic wetting approaches were performed with optical methods in order to directly observe the spontaneous spreading of a drop on model substrates. Less frequently, the dynamic meniscus was observed on vertical plates or cylinders pulled in or out of the liquids. Few studies make use the Wilhelmy method for dynamic tests and interpretation with dynamic models [23,24]. Moreover, it is important to observe that all these methods, to the best of our knowledge, were usually employed at room temperature with some well-known test liquids that are totally wetting. Such liquids include hexadecane [25], dodecane [14], methanol [20], ethanol [20] and especially polydimethylsiloxane (PDMS) [17,23,26,14] due to ease of obtaining PDMS oils of different viscosities. One recent study considers wetting of molten thermoplastics [27], but still in a spontaneous drop spreading configuration on glass substrates, that could not represent forced dynamic wetting conditions on fibres during composite manufacturing [28].

In this work, a procedure applicable to fibres and polymers was set in order to identify key parameters affecting dynamic wetting for composite manufacturing with molten polymers. A specific focus on the effect of temperature was made by varying the temperature between 25 °C and 75 °C. Cellulosic films were chosen as model cellulosic surfaces and two paraffin oils with different viscosity were selected as test liquids. The surface topography of films was evaluated using atomic force microscopy (AFM) whereas their chemical and crystallographic nature were characterised by Fourier-transform infrared spectroscopy (FTIR) and wide-angle X-ray diffraction (WAXD). Surface tensions of paraffin oils at different temperatures were measured by an optical method known as axisymmetric drop shape analysis (ADSA) and viscosity measurements were carried out with a rheometer. Forced dynamic wetting experiments were then performed at different temperatures and velocities with a weight tensiometer, according to the Wilhelmy method. Dynamic contact angles were expressed as a function of v and Ca and the plots were fitted using the HD theory. A discussion was conducted about the domain of validity and the physical significance of the cutoff parameters included in the Cox-Voinov law. Results show the relative importance of the influence of various parameters related to the processing conditions (temperature, velocity), to the liquid (viscosity, molecular weight) and to the solid/liquid interactions (contact angles) affecting the impregnation of fibrous reinforcements in composite processing. The contribution of this work also aims at finding physical parameters of dynamic wetting such as a slip length [29], a meaningful parameter that could be inserted into numerical models used to simulate flow processes.

2. Hydrodynamic (HD) theory

In this work a hydrodynamic approach was adopted to study the dynamic wetting in terms of dynamic contact angles (θ_d) versus capillary number (Ca). θ_d determined by the Wilhelmy weight method are defined as "apparent" contact angles, since measurements were carried out at a macroscopic scale and not at a local microscopic scale [17,19,30]. Moreover, the use of the HD theory is justified by the Ca range covered in this work, with most Ca above values for which the MK theory is usually found to be valid [20]. This result can be explained by the quite high viscosity of paraffin oils along with their low surface tensions and their totally wetting behaviour (for low velocities $\theta_d \approx$ °0). Therefore, since composite processing usually involves highly viscous molten polymers, the viscous dissipation channel is of particular interest in this particular framework.

According to the HD theory, a visco-capillary balance is made. The triple line was considered a liquid wedge with a corner flow. The contact angles were assumed to be small (θ_d [rad] ≪ 1) to take into account the lubrication approximation [31,32]. Assuming that the local velocity had a parabolic profile (Poiseuille profile), an average velocity of the triple line v was obtained. The viscous force was then defined as follows:

$$F_v = \frac{3\eta v}{\theta_d} \int \frac{dx}{x} \tag{2}$$

where x is the distance to the contact line [33–35]. To integrate this energy dissipation, two cut-off lengths had to appear, x_{max} and x_{min}:

$$F_v = \frac{3\eta v}{\theta_d} \ln\left(\frac{x_{max}}{x_{min}}\right) \tag{3}$$

The driving force for dynamic wetting, named as the out-of-balance capillary Young force, was instead defined as follows:

$$F_c = \gamma_{LV}(\cos(\theta_d) - \cos(\theta_e)) \tag{4}$$

with θ_e the equilibrium contact angle for an ideal surface at stable conditions. θ_e is approximately 0° for a total wetting and different from 0° for a partial wetting. In the reality, for $v = 0$ there is an hysteresis between a static advancing contact angle $\theta_{a\,s,}$ and a static receding contact angle $\theta_{r\,s,}$ [36,19]. Anyway, from the equivalence between the driven force F_c and the dissipation term F_v, the de Gennes law was obtained [35]:

$$\theta_d(\theta_d^2 - \theta_e^2) = 6ln\left(\frac{x_{max}}{x_{min}}\right)\frac{\eta v}{\gamma_{LV}} = 6\Gamma Ca \tag{5}$$

with:

$$\Gamma = \ln\left(\frac{x_{max}}{x_{min}}\right) \tag{6}$$

x_{max} was defined by de Gennes [12] as in the order of the capillary length k^{-1} (≈ 10^{-3} m), beyond which capillary effects are not meaningful:

$$k^{-1} = \sqrt{\frac{\gamma_{LV}}{\rho g}} \tag{7}$$

where ρ is the liquid density and g the acceleration of gravity. x_{min} was defined as a length in the order of the characteristic molecular size ($a \approx 10^{-9}$ m), named in several studies as a "slip length" [22]. Γ seems then to be exclusively a characteristic of liquid properties according to the hydrodynamic approach, and experimental studies found a range of Γ approximately between 10 and 20 for total wetting liquids [35,37,38]. However, the physical significance of Γ and particularly of the slip length x_{min} was questioned, because this value was sometimes observed less than atomic or molecular dimensions [25,20].

The de Gennes law (Eq. (5)) was generalised to flows with large contact angles by Cox and Voinov [33,34]. Revealing the viscous bending interface and integrating Stokes equations [13] they derived a similar polynomial law:

$$\theta_d^3 - \theta_e^3 = 9ln\left(\frac{x_{max}}{x_{min}}\right)\frac{\eta v}{\gamma_{LV}} = 9\Gamma Ca \tag{8}$$

It is important to observe that, when a liquid is totally wetting as paraffin oils, θ_e or more precisely for real cases $\theta_{a\,s,} \approx \theta_{r\,s,}$ will be considered 0° in these laws. Therefore, the dependence of θ_d on velocity with a power law of exponent 1/3 still appear valid. This power law dependence was experimentally proved for the first time by Hofmann [39] in advancing mode, and Cox-Voinov model was largely employed to predict dynamic wetting phenomena with the hydrodynamic approach. This law (Eq. (8)) will be then considered to fit experimental data of θ_a vs Ca. In regard to the receding mode (dewetting), the literature shows a transition from a partial wetting case to the total one at a entrainment threshold of velocity [31]. Beyond the velocity threshold, the formation of a thin liquid film occurs. The thickness of the liquid film will increase with the pull-out velocity, as described by the LandauLevich model [23,26].

3. Materials

3.1. Cellulosic films

To analyse the wetting of a plant fiber, cellulosic films, referenced as NatureFlex™ 23 NP and provided by Innovia films, were used in this study. Films have a thickness of 23µm and are manufactured from biodegradable cellulose, which is derived from wood pulp. Before wetting tests, cellulosic films were immersed for 1 h in ethanol, to remove the glycerol on surface that had the function of plasticizer, and then they were air-dried at ambient conditions (23 °C, 50% RH). Films were then cut to a length of 20 mm in the immersion direction and to a width of 10 mm in the transverse direction. These dimensions were found satisfying to perform immersion-withdrawal cycles (Section 4.3) without bending the films (Fig. 1).

3.2. Paraffin oils

Liquids used in this study were two paraffin oils. A paraffin oil (1) was provided by ACROS ORGANICS (Ref. 171400010, MP = −24 °C, BP =300 °C). Another one, paraffin oil (2), was provided by MERCK (Ref. 107160, MP = −12 °C, BP = 300 °C). Paraffin oils, like all alkanes, are made of saturated aliphatic carbon chains that are non polar, resulting in totally wetting liquids that do not react with cellulosic solid surfaces [40]. Their surface tension, density and viscosity were measured as a function of temperature (Sections 4.2.1 and 4.2.2).

4. Methods

4.1. Solid surface analysis

4.1.1. AFM

Atomic force microscopy (AFM) was performed on a Brüker INNOVA in contact mode, using TESPA tips (f≈ 320 kHz). Only samples obtained after glycerol removal were analysed to produce topographical data. Films were bound to the sample holder using double sided-tape. Prior to roughness calculation, the data were sequentially flattened using a plane fit model of the 0^{th}, 1 , $2^{st\,nd}$ and 3^{rd} order.

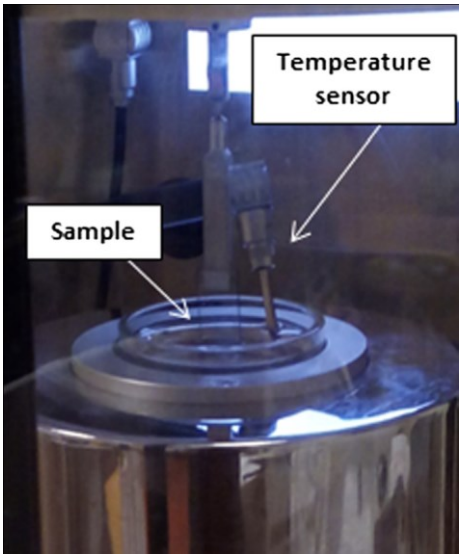

Fig. 1. Sample of cellulosic film in the K100SF tensiometer during a dynamic wetting test. (For interpretation of the references to color in this figure legend, the reader is referred to the web version of this article.)

Arithmetic roughness (R_a), geometric roughness (R_q) and maximum roughness (R_{max}) were then determined.

4.1.2. ATR-FTIR

Fourier-transform infrared spectroscopy (FTIR) measurements were done directly on the films with the help of a diamond attenuated total reflectance (ATR) accessory on a Perkin Elmer Frontier spectrometer. The data were averaged over 16 runs with a resolution of 4cm^{-1} in the 4000–650cm^{-1} region and three measurements were performed for each sample.

4.1.3. WAXD

Wide-angle X-ray diffraction (WAXD) was performed in reflection on a Panalytical XPert powder diffractometer equipped with a CoK_α anode (λ =1.7903 Å) powered at 40 kV and 40 mA. The detector was a linear Pixel 1D detector equipped with 0.04 rad Soller slits. The scan was performed in the 10–50° range in steps of 0.0525°. The specimen was stacked between two kapton foils. The diffractogram was converted to the more traditional copper wavelength (λ = 1.5419 Å) for presentation purposes.

4.2. Liquid property analysis

4.2.1. Rheological tests

A Physica MCR 501 rheometer from Anton Paar was used to measure viscosity of paraffin oils as a function of temperature. The standard geometry used for these measurements was a cone/plate system. Preliminary tests were conducted varying the shear rate and assuring that liquids can be considered newtonian fluids for the range of tested velocities in dynamic wetting [30]. The shear rate was then set at 100s^{-1} and the temperature rate fixed at 0.01°C/s. Viscosity of paraffin oils was measured at temperatures from 20°C to 80°C. Two rheological tests for each liquid were performed in order to verify the repeatability.

4.2.2. Pendant and sessile drop tests

A Krüss DSA100 tensiometer equipped with a high-temperature dosing system (DO3241) and a high temperature chamber (TC21) was used to measure surface tension of paraffin oils as a function of temperature [41]. Images of the drops were acquired (as in Fig. 2(a)), and the data were then treated with the proprietary Drop Shape Analysis

1.92.1.1 software. The surface tensions were determined using the axisymmetric drop shape analysis from the fit of the drop profile, knowing the needle diameter and the liquid density [42,43].

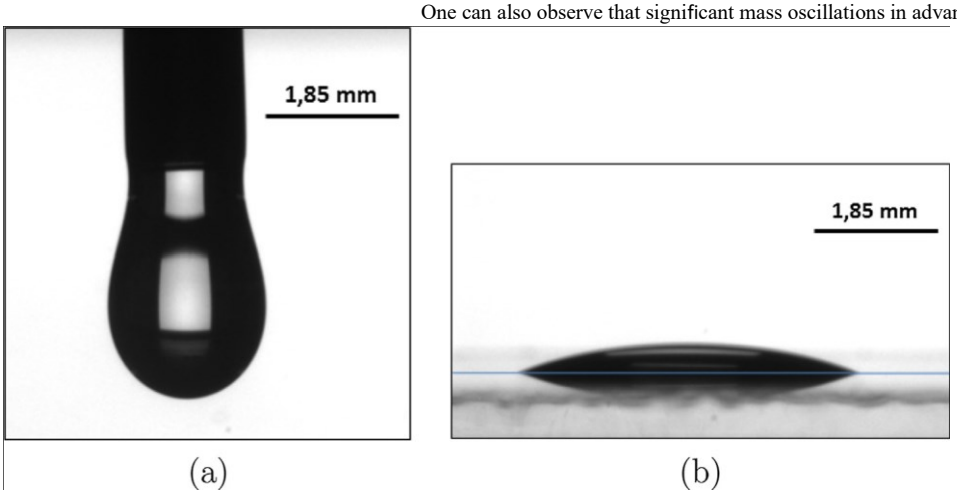

Fig. 2. (a) Pendant drop of paraffin oil (1) at T =75°C. (b) Sessile drop of paraffin oil (1) at 75°C on a glass slide. (For interpretation of the references to color in this figure legend, the reader is referred to the web version of this article.)

The needle used in this study had a diameter of 1.85 mm. Ten pendant drop tests were then performed at each temperature. In order to determine the densities of the polymers at all temperatures, volume measurements were conducted at different temperatures via the sessile drop method: sessile drops were deposited on a glass slide (Fig. 2(b)) and their volumes were measured by video means in triplicates. The weight of the drops were then measured using a balance in order to calculate the liquid density at each tested temperature. The surface tensions of the two paraffin oils were determined at 25, 50, 65, 75 and 85 °C. These tests also allowed to verify the stability of paraffin oils at high temperature versus the time scale of dynamic experiments, and that no evaporation or degradation could take place.

4.3. Dynamic wetting tests: the Wilhelmy method

A Krüss K100SF tensiometer with a temperature controller was used to perform dynamic wetting tests of the paraffin oils on the cellulosic substrates. Three temperatures were explored: 25, 50 and 75 °C. Different velocities were imposed for liquid immersion (wetting) and withdrawal (dewetting), from 1 mm/min to 500 mm/min. This protocol produced macroscopic dynamic contact angles for a large range of Ca [17].

In this method, the tensiometer measured the mass of liquid meniscus m formed on cellulosic film during a complete cycle of advancing, static and receding conditions. For each test, a cellulosic film was plunged in the liquid bath by the upward motion of the liquid vessel (advancing mode). The depth of immersion was set to 7 mm and the liquid vessel was placed manually close to the film, in order to make sure that a 3 mm immersion depth was always respected [44,45]. At the end of the immersion, the film was kept steady (static advancing conditions). Finally, it was withdrawn from the bath up to the initial position (receding mode). At the end of the cycle, the mass did not return to 0 since a residual liquid film remained on sample. This residual mass depends on the withdrawal velocity and could be described by the Landau-Levich model [23,26]. Buoyancy correction during advancing and receding can be neglected for films [44]. Corresponding advancing θ_a, static advancing $\theta_{a\,s,}$ and receding contact angles θ_r were derived from mass data via the Wilhelmy equation:

$$F = mg = \gamma_{LV} p \cos\theta_d \quad (9)$$

where F is the capillary force and p the wetted length.

Fig. 3 shows tensiometric curves obtained for three different imposed velocities of dynamic wetting test. As expected, hysteresis between advancing and receding was larger as velocity increased [19].

One can also observe that significant mass oscillations in advancing and receding modes were not found for these dynamic tests, demonstrating the strong triple line pinning/depinning marking the presence of heterogeneities [46,45]. This showed that surface of films could be approximated as a model substrate. Moreover for a quite ideal surface, the difference between the "quasi-static" advancing and receding contact angles (at very low speeds) has to be lower than 5° [23,18]. Tensiometric curves of dynamic wetting tests at low speeds (Fig. 3) confirmed that cellulosic films can be used as quite ideal surfaces. This assertion will be also confirmed by the solid surface characterisation in the next section.

5. Results and discussion

5.1. Solid surface characterisation

Fig. 4 shows a 3D rendering of typical surface topography of cellulosic films, obtained by AFM and Table 1 illustrates average and standard deviation values of arithmetic, geometric and maximal roughness.

It is possible to note that all roughness values were found lower than 100 nm, then roughness is well-below the range considered with the Cassie-Baxter and Wenzel models: 200 nm–30μm [47]. Therefore these surfaces were assumed as being smooth, such as model substrates.

Fig. 5 presents FTIR spectra for cellulosic films before and after ethanol treatment. The data were typical of cellulose II with –OH bands at 3440cm^{-1}, 3338cm^{-1}, a –CH stretching band at 2893cm^{-1} and the 1420cm^{-1} in-plane bending band of the hydroxyl group on the O(6) H. Glycerol removal by ethanol treatment was confirmed: disappearance of strong bands at 1659 and 1631cm^{-1} (water sorption), 1440cm^{-1} (CH_2 motion), 925cm^{-1} and 855cm^{-1} (fingerprint region)[48,49].

Regarding WAXD, typical cellulose II diffractograms with (110), ($1\bar{1}0$) and (020) peak contributions at $2.\theta \approx 13.2°$, 20.4° and 22.1° were observed (Fig. 6). The slight texture observed (lower intensity of the (110) signal) can be attributed to the orientation of the sample in the sample holder and to the well-known uniplanar orientation of cellulose [50,49].

Solid surface characterisation showed that the cellulosic films have not relevant physical and chemical heterogeneities and then, the hysteresis between advancing and receding in Fig. 3 depends only on the dynamic wetting and on

the liquid/solid interactions. Using natural fibres, the heterogeneous chemical composition of surface and the fibre morphology variability should have to be taken into account and correlated to the dynamic wetting.

5.2. Liquid viscosity and surface tension

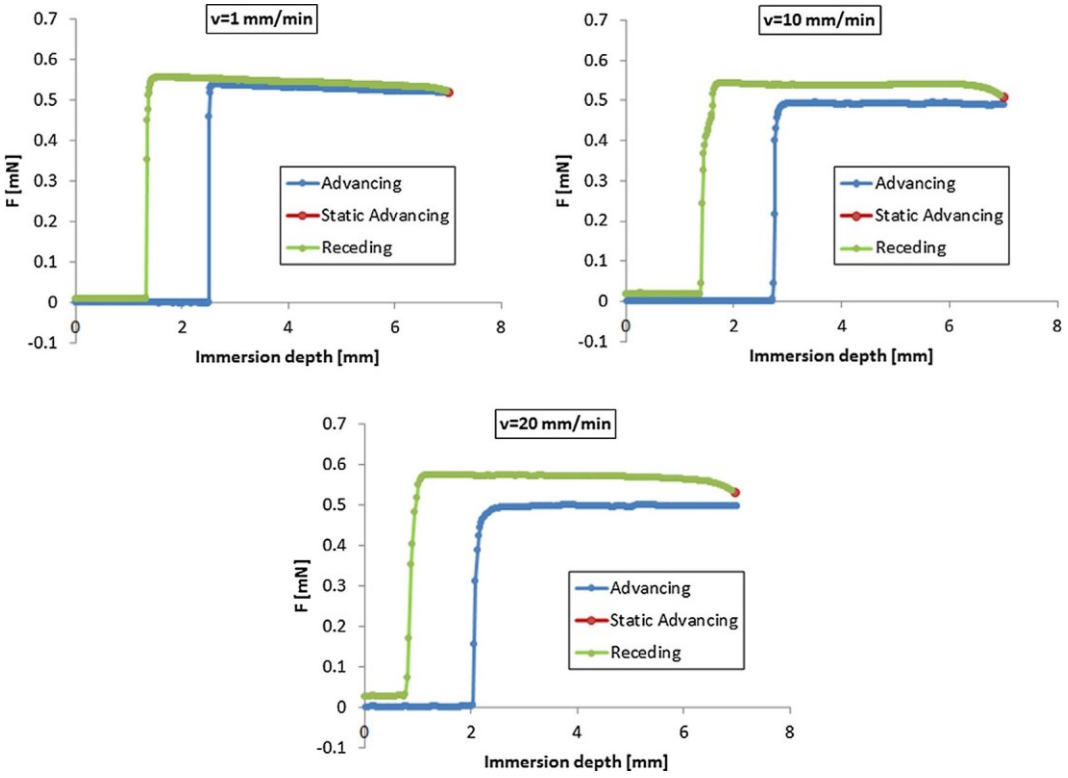

Fig. 3. Some tensiometric curves obtained by dynamic wetting tests at different v.

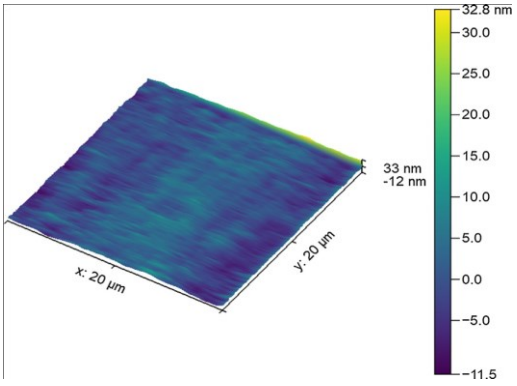

Fig. 4. Typical surface topography of the cellulosic substrate after ethanol treatment. (For interpretation of the references to color in this figure legend, the reader is referred to the web version of this article.)

Table 1
Arithmetic, geometric and maximum roughness calculated from AFM measurements.

	R_a (nm)	R_q (nm)	R_{max} (nm)
Mean	3.4	2.7	73.7
Standard deviation	1.3	1.2	27.6

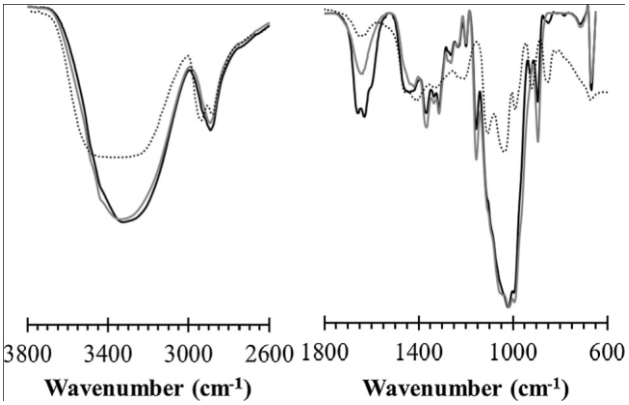

Fig. 5. FTIR transmittance spectra of the cellulosic films before (black line) and after (grey line) ethanol treatment. A standard glycerol curve (dotted line) is also displayed.

Viscosity η of paraffin oils as a function of temperature T are illustrated in Fig. 7. One can observe that the viscosities of paraffin oil (1) were higher than that of paraffin oil (2) at all temperatures. The temperature dependence of the viscosity was well-fitted with an Arrhenius plot, shown in Fig. 7, for both liquids. Then, viscosity values were determined at the three temperature conditions used for dynamic wetting tests. Table 2 shows these values, relevant to obtain capillary numbers (Eq. (1)).

Determined surface tensions γ_{LV} were plotted as a function of T, as shown in Fig. 8. The surface tensions decrease linearly with the increase in temperature, in accordance with the Eötvos law [51]. Moreover, this diminution

as a function of temperature is quite similar for the two liquids (the slope of linear trends is approximately the same), that is coherent with the fact that is the same type of liquid. Surface tension values of paraffin oil (1) are slightly higher than ones of paraffin oil (2), as in the case of viscosity. Table 3 shows results of density and surface tension at the three temperature conditions used for dynamic wetting analysis. Density values were employed for surface tension measurements, but also to calculate the capillary length (Eq. (7)) used as x_{max} in the Cox-Voinov law (Eq. (8)) (Table 4). Surface tension values are important for contact angles determination, but also to calculate capillary numbers (Eq. (1)).

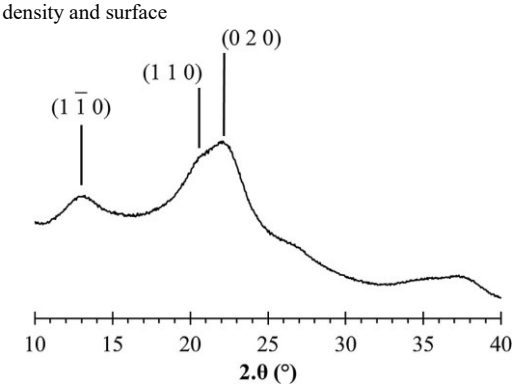

Fig. 6. X-ray diffraction pattern of the cellulosic film.

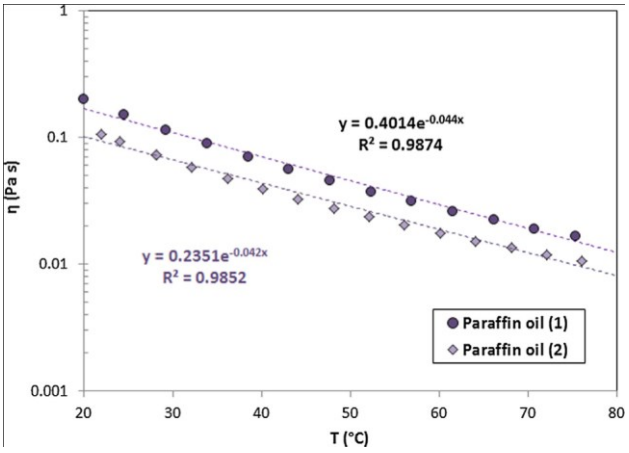

Fig. 7. Viscosity vs. temperature for paraffin oils.

Table 2
Viscosity results used for dynamic wetting study.

	η (Pa s) at 25 °C	η (Pa s) at 50 °C	η (Pa s) at 75 °C
Paraffin oil (1)	0.150± 0.006	0.044± 0.006	0.016± 0.006
Paraffin oil (2)	0.083± 0.003	0.029± 0.003	0.010± 0.003

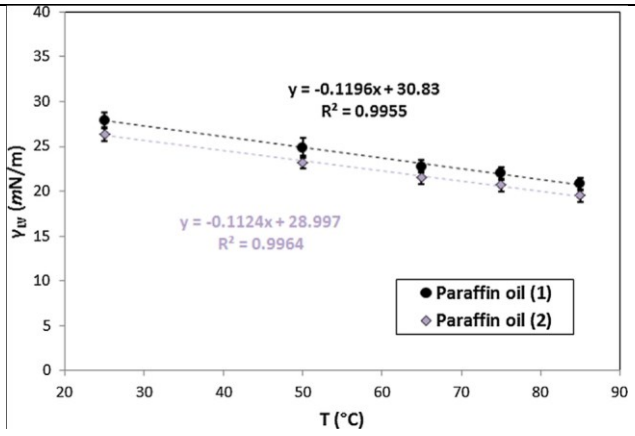

Fig. 8. Surface tension vs. temperature for paraffin oils. (For interpretation of the references to color in this figure legend, the reader is referred to the web version of this article.)

Table 3
Density and surface tension results used for dynamic wetting study.

T (°C)	Paraffin oil (1) ρ (g/cm)^3	Paraffin oil (1) γ_{LV}(mN/m)	Paraffin oil (2) ρ (g/cm)^3	Paraffin oil (2) γ_{LV}(mN/m)
25	0.88± 0.03	27.8± 0.8	0.89± 0.03	26.2± 0.7
50	0.86± 0.03	24.8± 1.1	0.85± 0.03	23.4± 0.7
75	0.83± 0.03	21.9± 0.7	0.82± 0.03	20.6± 0.7

Table 4
Capillary lengths and viscosity on surface tension ratios used for dynamic wetting study.

T (°C)	Paraffin oil (1) k^{-1} (mm)	Paraffin oil (1) (η/γ_{LV}) (s/m)	Paraffin oil (2) k^{-1} (mm)	Paraffin oil (2) (η/γ_{LV}) (s/m)
25	1.80± 0.17	5.38± 0.11	1.73± 0.20	3.17± 0.20
50	1.71± 0.34	1.73± 0.20	1.68± 0.29	1.24± 0.06
75	1.63± 0.23	0.77± 0.20	1.60± 0.24	0.49± 0.12

5.3. Advancing and receding contact angles

Three dynamic wetting tests were carried out for each velocity and temperature condition. From dynamic wetting tests via the Wilhelmy method, described at Section 4.3, advancing contact angles (θ_a), static advancing contact angles ($\theta_{a\,s,}$) and receding contact angles (θ_r) can be determined (Eq. (9)). These contact angles are "apparent" contact angles since they were obtained from macroscopic measurements [17]. Graphs of dynamic contact angle (θ_d) in advancing ($v > 0$) and receding ($v < 0$) modes as a function of imposed velocity v are shown in Figs. 9 and 10 for wetting of paraffin oil (1) and (2) respectively, at the three tested temperatures: 25, 50 and 75 °C.

Concerning advancing ($v > 0$), one can observe that for very low v (quasi-static advancing) the contact angles were found 0° at all temperature conditions, as expected for totally wetting liquids like paraffin oils. Advancing contact angles were found to be larger with the velocity increase. Moreover, the advancing contact angles were lowered by an increase in temperature at any given velocity. The temperature rise causes the decrease of liquid surface tension and density, and this could explain the decrease of contact angle values according to the Wilhelmy

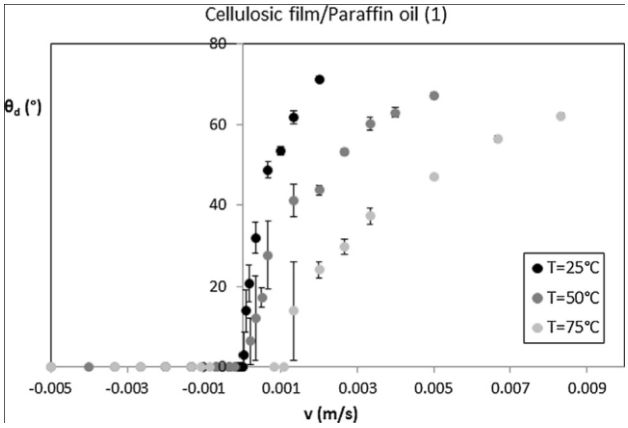

Fig. 9. Dynamic contact angles as a function of velocity for paraffin oil (1).

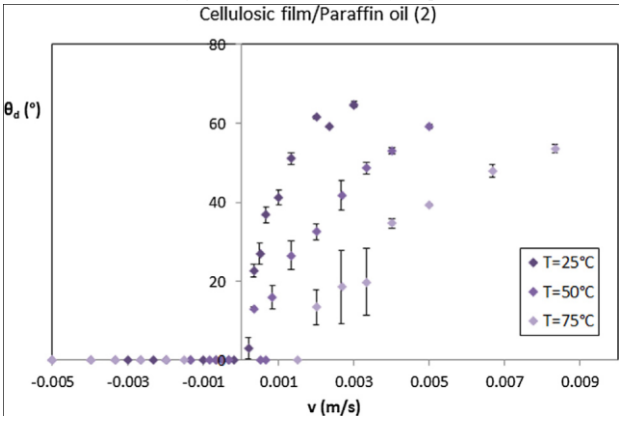

Fig. 10. Dynamic contact angles as a function of velocity for paraffin oil (2). (For interpretation of the references to color in this figure legend, the reader is referred to the web version of this article.)

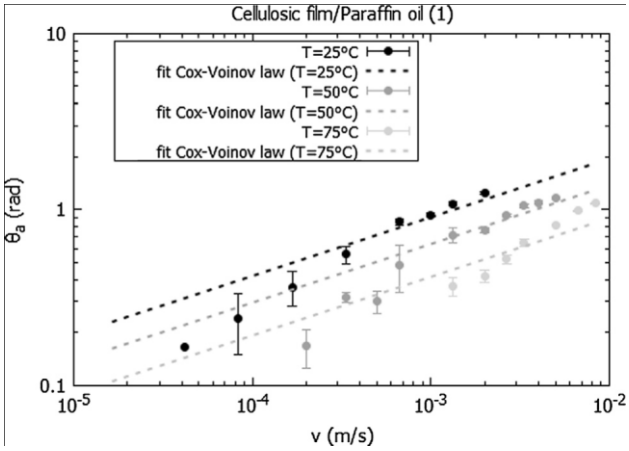

Fig. 11. Fits of experimental data of θ_a vs. v according to the Cox-Voinov model.

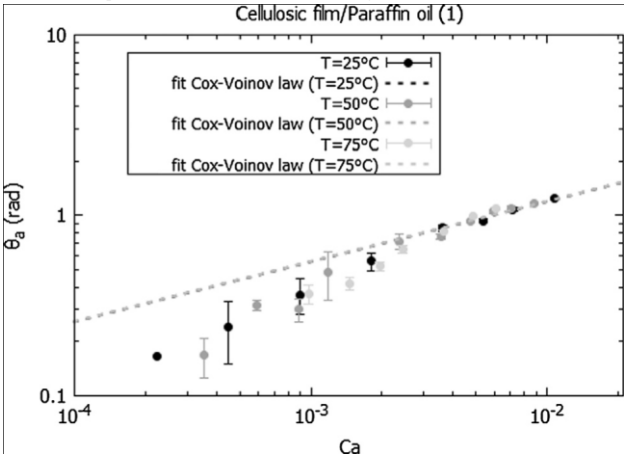

Fig. 12. Fits of experimental data of θ_a vs. Ca according to the Cox-Voinov model.

method. Figs. 9 and 10 show similar trends, given that liquid properties are similar. Advancing contact angles for paraffin oil (2) were slightly lower, due to its slightly lower surface tension. Advancing contact angles as a function of velocity seem to vary according to a power law at all temperatures. Data were then studied using the hydrodynamic approach represented by the Cox-Voinov law, in which the exponent of the power law is 1/3 (Eq. (8)).

Regarding receding ($v < 0$), angles were also found to be 0° for all velocities. This is coherent with the theory that, when total wetting transition appear ($\theta_d \approx$ °0), viscous dissipation as a function of velocity occurs in the residual liquid film on surface [23,26]. For total wetting liquids the transition occurs at quasi-static conditions. This result was found for both paraffin oils at all temperatures, indicating that it was relevant.

5.4. Prediction of dynamic wetting with the HD approach

To fit advancing contact angles with the Cox-Voinov law (Eq. (8)), θ_e was fixed to 0° (total wetting) and Γ (Eq. (6)) was the only free parameter in the model. Fig. 11 shows fit of θ_a versus v for cellulosic films with paraffin oil (1) at the three temperatures in a log–log scale plot. It is possible to note that the hydrodynamic model fits the experimental data well for high velocities at all temperatures. However, for low velocities a change of slope is observed. Viscous dissipation channel is dominant when viscosity and velocity are higher [20,18]. This explains the poor description of the data by the hydrodynamic theory as the velocity reaches low values or as the temperature increases (because of the viscosity decrease). Very similar results were observed for paraffin oil (2) (Fig. 10). As a consequence, the HD theory cannot be applied to the entire range of velocities.

Fig. 12 shows data for paraffin oil (1) as a function of Ca in a log–log scale plot. Capillary numbers were calculated via values of ($\eta\ \gamma/_{LV}$) in Table 4. This representation makes clear the effect of temperature on dynamic wetting. Varying the temperature modifies both surface tension and viscosity, changing the capillary number regime, but this temperature variation does not remarkably affect dynamic wetting behaviour of liquid on surface: the experimental data follow a same trend at various temperatures. Similar results were found for paraffin oil (2). Another important observation from graph in Fig. 12 is that hydrodynamic model fits quite well experimental results of advancing contact angles (θ_a) at different temperatures above $Ca \approx 2 \cdot 10^{-3}$, in agreement with results found in literature [20]. Below this value another dynamic wetting behaviour was observed, that could be linked to another dominant dissipation channel, explaining the change of slope in the log–log scale trend. Here, the slope is representative of a power law with a superior exponent (≈ 1/2), that could be described with the molecular kinetic (MK) theory [22]. Both types of behaviour can occur during the infiltration of the molten polymer within a dry preform of complex structure. Further analysis of dynamic wetting for low Ca ($Ca < 10^{-3}$) will constitute a perspective of this work.

Since dynamic wetting behaviour is independent of temperature, values of Γ obtained from fits with Cox-Voinov law (for $Ca > 2 \cdot 10^{-3}$) do not change significantly with temperature, as it can be observed in Tables 5 and 6 for paraffin oil (1) and (2) respectively. Moreover, these results are in the same order of Γ obtained for total wetting liquids found in literature [12]. Γ shown in Tables 5 and 6 could provide values of slip length [22], that is in the order of liquid characteristic molecular size a [12,25]. This size for small molecules,

such as in the case of paraffin oil, can be theoretically estimated through the following formula [52,53]:

$$a_{theor} = \left(\frac{M_n}{\rho N_A}\right)^{1/3} \quad (10)$$

where M_n is the molecular weight and N_A the Avogadro number. Using Eq. (10) values of theoretical Γ_{theor} were determined for all temperatures conditions and both liquids, as shown in Tables 5 and 6 proving to be in accordance with results of Γ from fits of experiences, that is, quite constant varying temperature.

Table 5
Results of Γ from fits with Cox-Voinov law, the coefficient of determination R^2 and comparison with Γ_{theor} (considering the characteristic molecular size a_{theor}) for paraffin oil (1).

	Paraffin oil (1)			
T (°C)	Γ	$R2$	a_{theor} (m)	Γ_{theor}
25	19.0± 0.7	0.984	$7.967 \cdot 10^{-10}$	14.63
50	19.2± 1.1	0.965	$8.028 \cdot 10^{-10}$	14.57
75	19.2± 2.4	0.997	$8.124 \cdot 10^{-10}$	14.51

Table 6
Results of Γ from fits with Cox-Voinov law, the coefficient of determination R^2 and comparison with Γ_{theor} (considering the characteristic molecular size a_{theor}) for paraffin oil (2).

	Paraffin oil (2)			
T (°C)	Γ	R^2	a_{theor} (m)	Γ_{theor}
25	17.2 ± 1.2	0.943	$7.937 \cdot 10^{-10}$	14.59
50	15.5± 2.1	0.990	$8.060 \cdot 10^{-10}$	14.55
75	19.4± 2.3	0.996	$8.157 \cdot 10^{-10}$	14.49

6. Conclusion

In the present work a dynamic wetting and dewetting study was carried out to reveal the effect of temperature on dynamic wetting behaviour for composite processing. During composite manufacturing, impregnation phenomena are affected by capillary forces, usually expressed in a capillary pressure, where dynamic contact angles appear and they are dependent on process condition. Indeed, an experimental procedure suitable to be applied to fibres and liquids in temperature had to be set in order to assess the dependence of the dynamic contact angle on the liquid velocity. In order to validate this protocol and analyse the wetting of a plant fibre, the choice of cellulosic films with a controlled morphology and chemical composition was made. Characterisation of film surface by means of AFM, FTIR and WAXD was performed to confirm estimation of cellulosic films as model substrates. About liquids, paraffin oils known as totally wetting were chosen. Liquid density, surface tension and viscosity were measured as a function of temperature via drop tensiometric methods and rheological tests. Then dynamic contact angles were determined for a large range of capillary number by means of the Wilhelmy method, at three different temperature conditions: $T = 25, 50, 75$ C° . Advancing contact angles versus capillary number were well predicted by the hydrodynamic theory for $Ca > 2 \cdot 10^{-3}$ at different T. The effect of this key parameter was finally established: varying the temperature modifies both surface tension and viscosity, changing the capillary number regime, but this temperature variation does not remarkably affect the slip length, which is a characteristic of the liquid in the hydrodynamic approach. Coherent physical values were found, proving that the experimental procedure coupled with the hydrodynamic model could be used to investigate the effect of other key parameters, such as the degree of polymerisation of molten polymers, also meaningful for composite manufacturing. Moreover, these parameters could be inserted in physical and numerical models developed to predict flow processes in fibrous preforms. Results are then relevant for a better understanding of the influence of temperature, viscosity and liquid/solid interaction on the dynamic contact angles and then on the dynamic wetting of a fibrous reinforcement by a polymer during LCM processes.

Acknowledgements

The authors would like to thank Dr. Jorge Peixinho (LOMC) for his kind assistance in rheological measurements and Isabelle Thielen (Innovia films) for kindly supplying the regenerated cellulose samples.

References

[1] Michaud V, Mortensen A. Infiltration processing of fibre reinforced composites: governing phenomena. Compos Part A: Appl Sci Manuf 2001;32(8):981–96.
[2] Salvatori D, Caglar B, Teixidó H, Michaud V. Permeability and capillary effects in a channel-wise non-crimp fabric. Compos Part A: Appl Sci Manuf 2018;108:41–52.
[3] Verrey J, Michaud V, Månson J-A. Dynamic capillary effects in liquid composite moulding with non-crimp fabrics. Compos Part A: Appl Sci Manuf 2006;37(1):92–102.
[4] Pucci MF, Liotier P-J, Drapier S. Capillary wicking in a fibrous reinforcement–orthotropic issues to determine the capillary pressure components. Compos Part A: Appl Sci Manuf 2015;77:133–41.
[5] Bréard J, Henzel Y, Trochu F, Gauvin R. Analysis of dynamic flows through porous media. part i: Comparison between saturated and unsaturated flows in fibrous reinforcements. Polym Compos 2003;24(3):391–408.
[6] Leclerc JS, Ruiz E. Porosity reduction using optimized flow velocity in resin transfer molding. Compos Part A: Appl Sci Manuf 2008;39(12):1859–68.
[7] Lundström TS, Gustavsson LH, Jēkabsons N, Jakovics A. Wetting dynamics in multiscale porous media. porous pore-doublet model, experiment and theory. AIChE J 2008;54(2):372–80.
[8] Wielhorski Y, Ben Abdelwahed MA, Bizet L, Bréard J. Wetting effect on bubble shapes formed in a cylindrical t-junction. Chem Eng Sci 2012;84:100–6.
[9] Ben Abdelwahed MA, Wielhorski Y, Bizet L, Bréard J. Bubble formation and transport in t-junction for application to liquid composite molding: Wetting effect. J Compos Mater 2014;48(1):37–48.
[10] Celle P, Drapier S, Bergheau J-M. Numerical modelling of liquid infusion into fibrous media undergoing compaction. Eur J Mech-A/Solids 2008;27(4):647–61.
[11] Park CH, Lebel A, Saouab A, Bréard J, Lee WI. Modeling and simulation of voids and saturation in liquid composite molding processes. Compos Part A: Appl Sci Manuf 2011;42(6):658–68.
[12] de Gennes P-G, Brochard-Wyart F, Quéré D. Capillarity and wetting phenomena: drops, bubbles, pearls, waves. Springer Science & Business Media; 2013.
[13] Snoeijer JH, Andreotti B. Moving contact lines: scales, regimes, and dynamical transitions. Ann Rev Fluid Mech 2013;45.
[14] Mohammad Karim A, Davis S, Kavehpour H. Forced versus spontaneous spreading of liquids. Langmuir 2016;32(40):10153–8.
[15] Pillai KM, Advani SG. Wicking across a fiber-bank. J Colloid Interface Sci 1996;183(1):100–10.
[16] Masoodi R, Pillai KM. Darcy's law-based model for wicking in paper-like swelling porous media. AIChE J 2010;56(9):2257–67.
[17] Sauer BB, Kampert WG. Influence of viscosity on forced and spontaneous spreading: Wilhelmy fiber studies including practical methods for rapid viscosity measurement. J Colloid Interface Sci 1998;199(1):28–37.
[18] Bonn D, Eggers J, Indekeu J, Meunier J, Rolley E. Wetting and spreading. Rev Mod Phys 2009;81(2):739.
[19] Blake TD. The physics of moving wetting lines. J Colloid Interface Sci 2006;299(1):1–13.

[20] Petrov JG, Ralston J, Schneemilch M, Hayes RA. Dynamics of partial wetting and dewetting in well-defined systems. J Phys Chem B 2003;107(7):1634–45.
[21] Petrov P, Petrov I. A combined molecular-hydrodynamic approach to wetting kinetics. Langmuir 1992;8(7):1762–7.
[22] Seveno D, Vaillant A, Rioboo R, Adao H, Conti J, De Coninck J. Dynamics of wetting revisited. Langmuir 2009;25(22):13034–44.
[23] Maleki M, Reyssat E, Quéré D, Golestanian R. On the landau- levich transition. Langmuir 2007;23(20):10116–22.
[24] Iliev SD, Pesheva NC. Dynamic meniscus profile method for determination of the dynamic contact angle in the wilhelmy geometry. Colloids Surf A: Physicochem Eng Aspects 2011;385(1-3):144–51.
[25] Schneemilch M, Hayes RA, Petrov JG, Ralston J. Dynamic wetting and dewetting of a low-energy surface by pure liquids. Langmuir 1998;14(24):7047–51.
[26] Maleki M, Reyssat M, Restagno F, Quéré D, Clanet C. Landau–levich menisci. J Colloid Interface Sci 2011;354(1):359–63.
[27] Zhang Y, Fuentes CA, Koekoekx R, Clasen C, Van Vuure AW, De Coninck J, et al. Spreading dynamics of molten polymer drops on glass substrates. Langmuir 2017;33(34):8447–54.
[28] Binetruy C, Pabiot J, Hilaire B. The influence of fiber wetting in resin transfer molding: scale effects. Polym Compos 2000;21(4):548–57.
[29] Yeager M, Advani SG. Numerical model of fiber wetting with finite resin volume. Integrat Mater Manuf Innovat 2015;4(1):3.
[30] Min Q, Duan Y-Y, Wang X-D, Liang Z-P, Si C. Does macroscopic flow geometry influence wetting dynamic? J Colloid Interface Sci 2011;362(1):221–7.
[31] Brochard-Wyart F, de Gennes P. Dynamics of partial wetting. Adv Colloid Interface Sci 1992;39:1–11.
[32] Lu G, Wang X-D, Duan Y-Y. A critical review of dynamic wetting by complex fluids: from newtonian fluids to non-newtonian fluids and nanofluids. Adv Colloid Interface Sci 2016;236:43–62.
[33] Cox B. On driving a viscous fluid out of a tube. J Fluid Mech 1962;14(1):81–96.
[34] Voinov O. Hydrodynamics of wetting. Fluid Dyn 1976;11(5):714–21.
[35] de Gennes P-G. Wetting: statics and dynamics. Rev Mod Phys 1985;57(3):827.
[36] Le Grand N, Daerr A, Limat L. Shape and motion of drops sliding down an inclined plane. J Fluid Mech 2005;541:293–315.
[37] Marsh JA, Garoff S, et al. Dynamic contact angles and hydrodynamics near a moving contact line. Phys Rev Lett 1993;70(18):2778.
[38] Bico J, Quere D. Liquid trains in a tube. EPL (Europhys Lett) 2000;51(5):546.
[39] Hoffman RL. A study of the advancing interface. I. interface shape in liquid-gas systems. J Colloid Interface Sci 1975;50(2):228–41.
[40] Saito M, Yabe A. Dispersion and polar force components of surface tension of some polymer films. Text Res J 1983;53(1):54–9.
[41] Berry JD, Neeson MJ, Dagastine RR, Chan DY, Tabor RF. Measurement of surface and interfacial tension using pendant drop tensiometry. J Colloid Interface Sci 2015;454:226–37.
[42] Song B, Springer J. Determination of interfacial tension from the profile of a pendant drop using computer-aided image processing: 1. theoretical. J Colloid Interface Sci 1996;184(1):64–76.
[43] Song B, Springer J. Determination of interfacial tension from the profile of a pendant drop using computer-aided image processing: 2. experimental. J Colloid Interface Sci 1996;184(1):77–91.
[44] Pucci MF, Liotier P-J, Drapier S. Tensiometric method to reliably assess wetting properties of single fibers with resins: Validation on cellulosic reinforcements for composites. Colloids Surf A: Physicochem Eng Aspects 2017;512:26–33.
[45] Pucci MF, Liotier P-J, Seveno D, Fuentes C, Van Vuure A, Drapier S. Wetting and swelling property modifications of elementary flax fibres and their effects on the liquid composite molding process. Compos Part A: Appl Sci Manuf 2017;97:31–40.
[46] Duursma G, Sefiane K, David S. Advancing and receding contact lines on patterned structured surfaces. Chem Eng Res Des 2010;88(5):737–43.
[47] Quéré D. Wetting and roughness. Annu Rev Mater Res 2008;38:71–99.
[48] Nelson ML, O'Connor RT. Relation of certain infrared bands to cellulose crystallinity and crystal latticed type. part I. spectra of lattice types i, ii, iii and of amorphous cellulose. J Appl Polym Sci 1964;8(3):1311–24.
[49] Duchemin B. Mercerisation of cellulose in aqueous naoh at low concentrations. Green Chem 2015;17(7):3941–7.
[50] Zugenmaier P. Conformation and packing of various crystalline cellulose fibers. Progress Polym Sci 2001;26(9):1341–417.
[51] Moreira JC, Demarquette NR. Influence of temperature, molecular weight, and molecular weight dispersity on the surface tension of ps, pp, and pe. i. experimental. J Appl Polym Sci 2001;82(8):1907–20.
[52] Brochard F, de Gennes P. Shear-dependent slippage at a polymer/solid interface. Langmuir 1992;8(12):3033–7.
[53] Lhermerout R, Perrin H, Rolley E, Andreotti B, Davitt K. A moving contact line as a rheometer for nanometric interfacial layers. Nature Commun 2016;7:12545.